IMPACT OF LEARNING SET AND SAMPLING FOR SNOW AVALANCHE SUSCEPTIBILITY MAPPING WITH RANDOM FOREST

S. Cetinkaya[1,2], S. Kocaman [2]*

[1] Hacettepe University, Graduate School of Science and Engineering, Ankara, Türkiye – sinemcetinkaya@hacettepe.edu.tr
[2] Dept. of Geomatics Engineering, Hacettepe University, 06800 Beytepe Ankara, Türkiye - sultankocaman@hacettepe.edu.tr

KEY WORDS: Snow avalanche susceptibility, snow avalanche inventory, random forest, remote sensing, machine learning

ABSTRACT: Snow avalanche refers to rapid snow mass movement under the influence of gravity and is a frequently observed natural phenomenon in mountainous regions. An area affected by a snow avalanche consists of starting, track (or transition) and runout (or deposition) zones, which have different geomorphologic characteristics that need to be considered in hazard modelling. This study attempted to analyze the impact of the different zones in producing snow avalanche susceptibility maps (ASMs) with data-driven methods. The random forest (RF) method was applied to the data from Gross Spannort Mountain region (Switzerland) for this purpose. Avalanche inventories from two dates were manually delineated to separate the three zones and two RF models were trained with learning datasets; i.e. Inventory-A which includes all snow avalanche zones (original inventory), and Inventory-B with starting and track zones. The conditioning factors were defined based on the literature, data availability and study area characteristics. The trained models (Model-A with Inventory-A and Model-B with Inventory-B) were evaluated with the area under the receiver operating characteristic (ROC), precision, recall and F1 score. The results show that Model-A has AUC of 0.97, precision of 0.89, recall of 0.95 and F1 score of 0.92 and the Model-B has AUC of 0.98, precision of 0.90, recall of 0.94 and F1 score of 0.92 that indicate high prediction performances for both cases. Furthermore, feature importance values were calculated by the Mean Decrease in Impurity (MDI) method, and elevation, aspect and valley depth were found the most influencing conditioning factors.

1. INTRODUCTION

Snow avalanches can be defined as rapid mass movement of snow, ice, rock and soil on snow covered steep slopes. Snow avalanche occurs depending on terrain, meteorological and snowpack properties (Schweizer et al., 2003). A snow avalanche may contain soil, rocks, vegetation, or ice particles, all of which can have profoundly devastating socioeconomic and environmental effects. Snow avalanche susceptibility assessment is crucial for disaster management to identify the spatial probability distribution of hazard-prone areas.

An area affected by a snow avalanche event consists of three sub-regions, such as starting, track and runout zones. An avalanche initiates from the starting zone, where unstable snow originates and then flows through the track to the runout zone. Delineation of avalanche zones, especially starting and runout zones, plays a crucial role for avalanche hazard and risk assessments (Bianchi et al., 2021; Beato Bergua et al., 2019; Chueca Cía et al., 2014; Fazzini et al., 2021; Kim & Park, 2017; Meseșan et al., 2019). The characteristics of starting zone and track can influence the size and speed of avalanche, which in turn affects runout zone. The distribution of snow mass in the runout zone and starting zone can be used for predicting potential damage to buildings and infrastructures (Cappabianca et al., 2018; Pistocchi & Notarnicola, 2013). The geomorphologic characteristics of each zone differ significantly from each other, and they should be considered for accurate avalanche hazard modeling (Choubin et al., 2019).

In recent decades, Geographic Information Systems (GIS) and remote sensing (RS) domains have provided important tools for enabling improved disaster management. Data-driven machine learning (ML) techniques have contributed to numerous natural hazard assessment studies. Recently, several snow avalanche susceptibility studies have been conducted with the ML algorithms such as Support vector machine (SVM), K-nearest neighbours (KNN), Classification and Regression Tree (CART), Multilayer perceptron (MLP), Logistics Regression (LR), Random Forest (RF), and others (Akay, 2021; Rahmati et al., 2019; Tiwari et al., 2021; Wen et al., 2022).

Here, we employed a widely used ML algorithm, the RF, to generate two snow avalanche susceptibility maps (ASMs) for the Gross Spannort Mountain region (Switzerland). A previous study was carried out for producing the ASM for Davos, Switzerland by employing a set of features (partly different from the present study) using the RF and LR methods (Cetinkaya and Kocaman, 2022), which illustrated higher prediction quality of the RF classifier. The present research aimed to provide a better insight into the impact of learning sample selection on snow avalanche susceptibility mapping, by investigating in particular the use of runout zones for this purpose. After a literature survey on the regional characteristics and snow susceptibility assessment studies, a total of 18 features were utilized as conditioning factors that are elevation, slope, land use and land cover (LULC), diurnal anisotropic heating index (DAH), plan curvature, profile curvature, aspect, relative slope position index (RSP), slope length factor (LS), topographic position index (TPI), topographic ruggedness index (TRI), topographic wetness index (TWI), convergence index, wind exposition index (WEI), mid-slope position index (MSP), valley depth (VD), normalized height, and lithology. A snow avalanche inventory produced by (Hafner & Bühler, 2019) was provided as 2D polygons and employed here for learning. In addition, the prediction capabilities of the methods were analyzed using the

* Corresponding author

area under the receiver operating characteristic (ROC) curve (AUC), precision, recall, and F1 score. Furthermore, the influence of the conditioning factors on the models was evaluated with feature importance analysis and presented here.

2. MATERIALS AND METHODS

2.1 Study Area

The study region is located between Erstfeld and Engelberg in Central Switzerland and covers an area of 259 km^2 (Figure 1). Gross Spannort Mountain, part of the Uri Alps, is the highest point of the investigated area with an altitude of 3,198 meters at the peak. Avalanches occur frequently in the region, and the site was selected due to the accurate and reliable inventory.

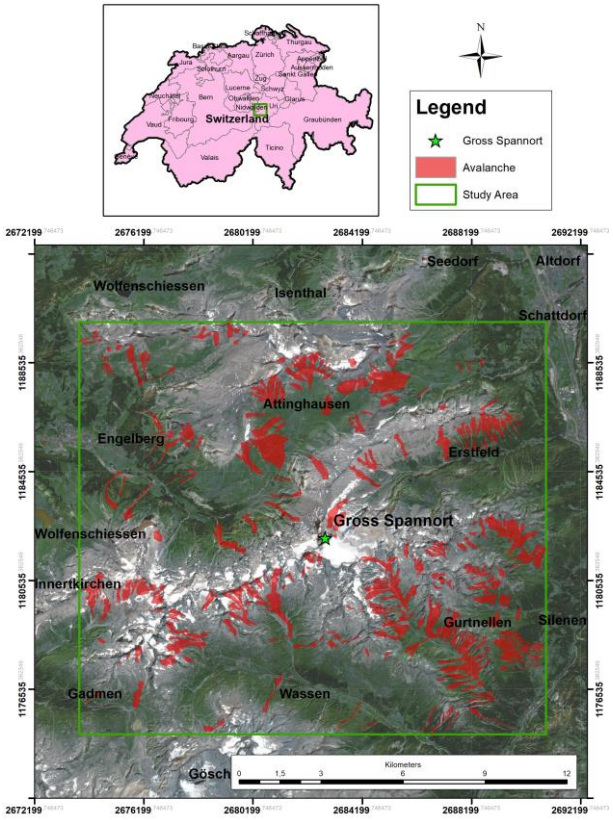

Figure 1. Location of the study area.

2.2 Input Datasets and Features

Here, we aimed to investigate the impact of inventory, in particular the use of different avalanche zones, on ASM production. Initially, the starting, track and runout zones of the avalanche polygons in the inventory data provided by Hafner & Bühler (2019) was manually delineated using a desktop GIS software. Thus, besides the original inventory with all zones (Inventory-A), a second map called Inventory-B involving only starting and track zones was produced. The number of pixels involved in both inventories is given in Table 1. The overall workflow of the study used to produce the ASMs is illustrated in Figure 2.

The digital elevation model (DEM), lithology and LULC of the study area were obtained from the Swiss Federal Office of Topography, Switzerland (Swisstopo, 2021). The conditioning factors, which are depicted in Figure 2 as numerical factors, were generated from DEM in the SAGA GIS environment (Conrad et al., 2015). The statistical summary of numerical factors can be found in Table A1 (Appendix). Both inventory maps and the feature maps representing the conditioning factors (see Figure A1 in Appendix) were converted into raster datasets with a dimension of 1518 x 1713 pixels and 10 m resolution.

	Inventory-A (Starting + Track + Runout Zones)	Inventory-B (Starting + Track Zones)
Avalanche	274,967	207,314
Non - Avalanche	2,325,367	2,393,020

Table 1. The pixel counts of snow avalanche inventories.

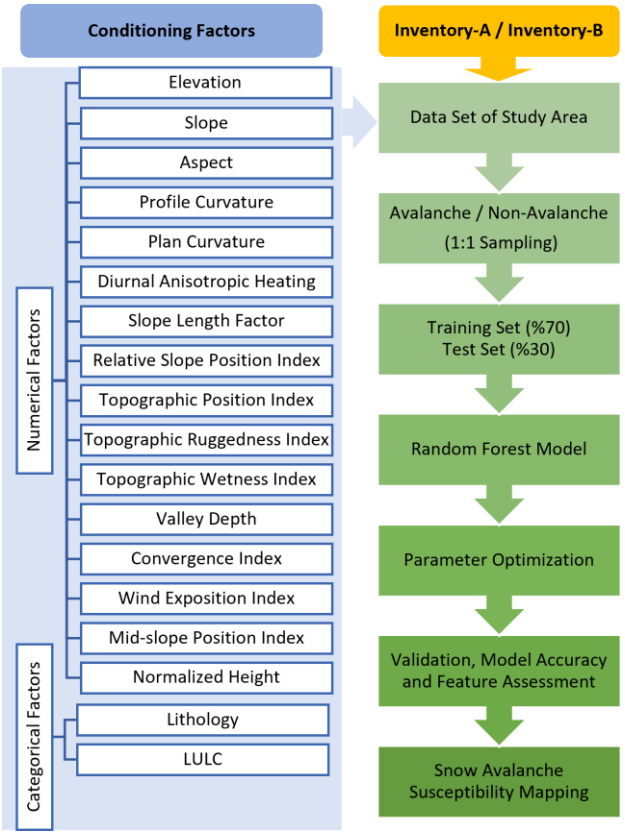

Figure 2. Snow avalanche susceptibility mapping workflow.

2.3 Snow Avalanche Susceptibility Mapping

In the current study, the random undersampling technique of SMOTE (Chawla et al., 2002) was used to handle an imbalanced dataset by random selection relying on avalanche inventories (by using a ratio of 1/1 for avalanche/non-avalanche pixels). The learning dataset was split as training (70%) and validation (30%) for producing the ASMs with Inventory-A and Inventory-B, separately. The parameter optimization strategy was conducted with existing libraries for the RF in a Python environment. The RF proposed by Breiman (2001) is one of the most widely used ML algorithms based on a large number of decision trees. It has the ability to reduce overfitting problems as well as to perform accurate classifications.

Parameter optimization plays a crucial role in the accuracy of ML algorithms. In this study, the HalvingGridSearchCV (Pedregosa et al., 2011) implemented in Scikit-learn library was applied to identify optimal parameters, which are given in Table

2. The area under the receiver operatic characteristic curve (AUC) was used to evaluate the model's predictive abilities. The performance assessment of the models was also investigated using precision, recall and F1-score values.

Parameters	Model-A	Model-B
Number of estimators	500	500
Max depth	32	32
Max feature	32	32
Min sample leaf	1	1
Min sample split	2	2

Table 2. Optimal parameters of RF models.

2.4 Feature Importance

Feature importance enables to compute of the relative importance of each feature in a predictive model. The Mean Decrease in Impurity (MDI) method was selected to measure the effects of each feature on the models. The higher the calculated value, the higher the contribution of the feature to the model is considered and vice versa.

3. RESULTS AND DISCUSSIONS

In this study, two ASMs were produced by using Inventory-A (all zones) and Inventory-B (without runout zone) with 18 conditioning factors by applying the RF model (hereinafter will be referred as Model-A and Model-B, respectively). As summarized in Table 3, the models achieved similarly accurate results in terms of precision, recall and F1 score, which indicate high coherence between the learning datasets and the models. The AUC values obtained from both models (Figure 3 and Figure 4) show that Model-B (AUC = 0.98) performed slightly better than Model-A (AUC = 0.97).

	Class	Precision	Recall	F1-Score
Model-A	**Non - Avalanche**	0.95	0.88	0.91
	Avalanche	0.89	0.95	0.92
Model-B	**Non - Avalanche**	0.94	0.90	0.92
	Avalanche	0.90	0.94	0.92

Table 3. Overall precision, recall, and F1-Score of the RF models.

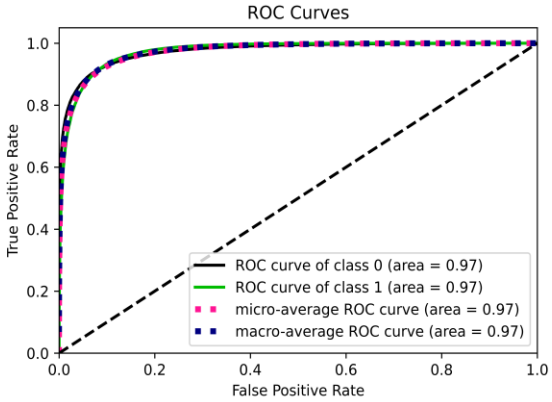

Figure 3. The ROC curve obtained from Model-A.

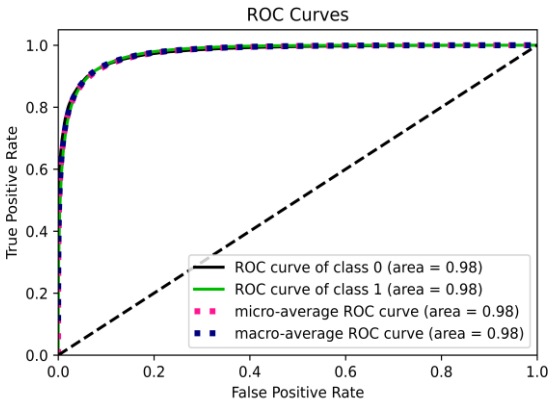

Figure 4. The ROC curve obtained from Model-B.

The feature importance results computed from the models are given in Figure 5. In the figure, the features ranked almost identically according to the importance values of the models. Both models indicated that the elevation is the most important variable, followed by aspect, valley depth, and wind exposition index. Based on the importance values of the elevation feature, Model-B indicated that elevation has even higher importance for modeling when runout zones are not considered. It can also be observed that DEM-derived features contribute to avalanche susceptibility greater than lithology and LULC in the site. Yet, a few lithology types such as serpentinite, talc schist, metaperidotite, and granite, granodiorite were found effective in learning.

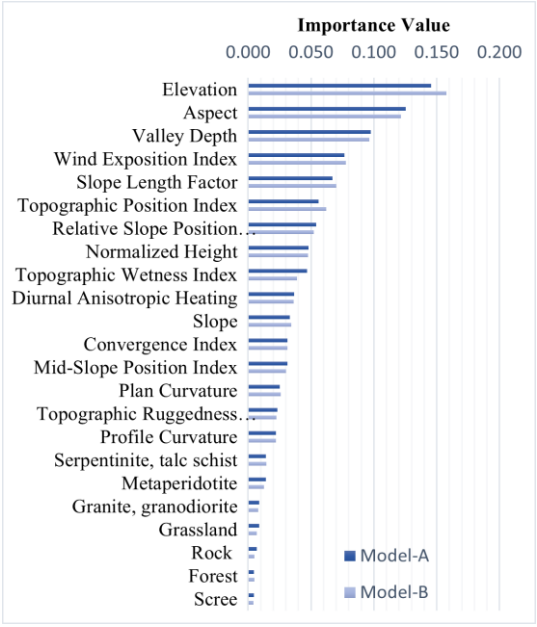

Figure 5. Feature importance of the RF models.

Figure 6 demonstrates the ASMs of the study area produced by the prediction results of the RF models and detailed views from different parts. Although the performance metrics calculated from Model-A and Model-B were quite similar, the spatial distribution of model probabilities differed significantly from each other (see Figure 6). Model-A identified larger areas as snow avalanche-prone than Model-B as expected.

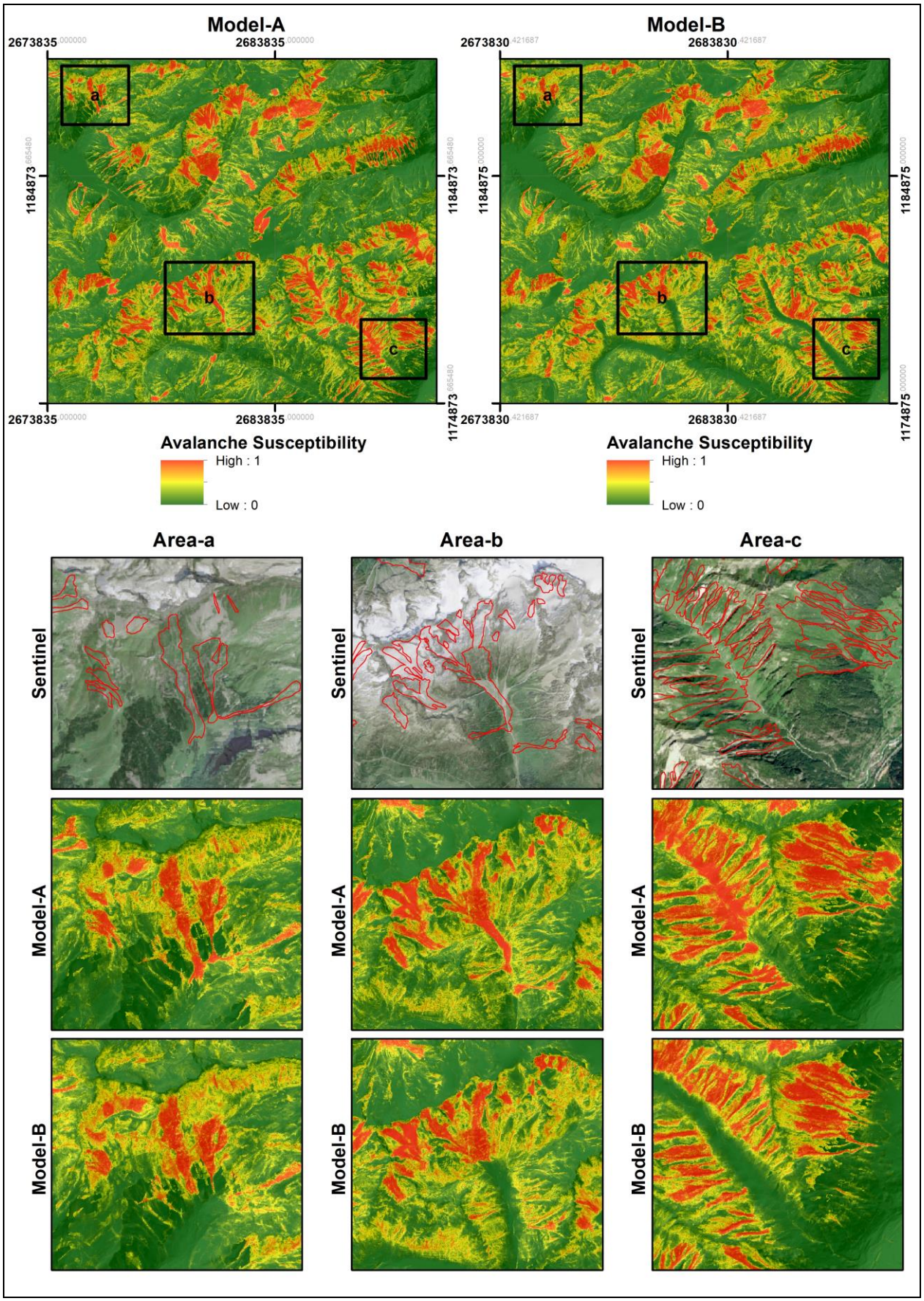

Figure 6. Snow avalanche susceptibility belongs to Model-A, and Model-B.

When the feature statistics given in Table A1 in Appendix is analyzed, it can be seen that removing runout zones from the inventory enabled a differentiation between the avalanche/non-avalanche zones in terms of elevation and its first derivative, the slope. In addition, the slope length factor and mid-slope position index varies between both inventories. Thus, removal of runout zones helped to better classify avalanche-non-avalanche zones. On the other hand, there are other features that keep the mean values even after the removal of runout zones, such as the aspect and wind exposition index, which are highly effective variables in both models. The detailed maps shown in Figure 6 for the three sub-areas as marked in the maps of the whole site indicate that both models can successfully classify the data for which they aim for, i.e. Model-A the avalanches with all zones, and Model-B the starting and the track zones. On the other hand, as mentioned previously, the characteristics of starting zone and track can influence the size and speed of avalanche, which in turn affects runout zone. Thus, the use purposes of both models would be different and an ASM should rather be produced by using the starting and track zones. Yet, the runout zones predicted by Model-A, which can precisely be delineated by differencing ASM-A and ASM-B, would be a good approximation for risk assessment under the given conditions of the avalanche periods mapped by Hafner and Bühler (2019).

4. CONCLUSIONS

Snow avalanches are among destructive natural hazards in cold and snow-covered mountainous regions. Within the scope of this study, the RF model was applied for the avalanche susceptibility mapping of an area in Gross Spannort Mountain region, Switzerland by using two types of avalanche inventory maps. Inventory-A includes avalanche polygons with the starting, track and runout regions delineated as a single zone for each event. Inventory-B includes the starting and runout zones (without runout zones) to assess the influence of the learning data on the produced ASMs. The results show that both models could successfully classify the data for the given inventory types with AUC values of 0.98 (Model-B) and 0.97 (Model-A). The results illustrate high performance of the RF models for snow avalanche hazard and risk assessments. The features employed for this purpose were also found suitable for precise modeling.

On the other hand, the use purpose of an ASM must clearly be defined and they should be produced based on it. In order to assess the avalanche susceptibility, starting and track zones need to be used as the runout zones depend on the characteristics of starting and track zones, which can influence the size and speed of avalanche. Yet, the results of Model-B also show that the RF can classify the runout zones when high quality data for all zones are available that can provide a good approximation for risk assessment under similar conditions.

In previous studies, applying elimination and backward selection of features would be another strategy to improve ASMs. Further research is necessary to demonstrate the ability of transfer learning. Apart from these, the inventory data was manually divided into avalanche zones in the study, which raises the question of whether we can obtain avalanche zones with ML methods.

ACKNOWLEDGEMENTS

The authors thank to Elisabeth Hafner, Dr. Yves Bühler and WSL Institute for Snow and Avalanche Research SLF, Switzerland for the provision of avalanche inventory data. This paper is part of the Ph.D. thesis research of Sinem Cetinkaya and was carried out with the support of Higher Education Council of Turkey (YÖK) within the 100/2000 Programme.

REFERENCES

Akay, H., 2021. Spatial modeling of snow avalanche susceptibility using hybrid and ensemble machine learning techniques. *Catena*, *206*. https://doi.org/10.1016/j.catena.2021.105524.

Breiman, L., 2001. Random forests. *Machine Learning*, *45*(1), 5–32. https://doi.org/10.1023/A:1010933404324.

Beato Bergua, S., Poblete Piedrabuena, M. Á., & Marino Alfonso, J. L., 2019. Snow avalanches, land use changes, and atmospheric warming in landscape dynamics of the Atlantic mid-mountains (Cantabrian Range, NW Spain). *Applied Geography*, 107, 38-50. https://doi.org/10.1016/j.apgeog.2019.04.007.

Bianchi, F. M., Grahn, J., Eckerstorfer, M., Malnes, E., & Vickers, H., 2021. Snow Avalanche Segmentation in SAR Images with Fully Convolutional Neural Networks. *IEEE Journal of Selected Topics in Applied Earth Observations and Remote Sensing*, 14, 75-82, https://doi.org/10.1109/JSTARS.2020.3036914.

Cappabianca, F., Barbolini, M., & Natale, L., 2008. Snow avalanche risk assessment and mapping: A new method based on a combination of statistical analysis, avalanche dynamics simulation and empirically-based vulnerability relations integrated in a GIS platform. *Cold Regions Science and Technology*, *54*(3), 193–205. https://doi.org/10.1016/j.coldregions.2008.06.005.

Cetinkaya, S., Kocaman, S., 2022. Snow Avalanche Susceptibility Mapping for DAVOS, Switzerland. *The International Archives of Photogrammetry, Remote Sensing and Spatial Information Sciences, 43*, 1083-1090. https://doi.org/10.5194/isprs-archives-XLIII-B3-2022-1083-2022.

Chawla, N.v, Bowyer, K. W., Hall, L. O., & Kegelmeyer, W. P., 2002. SMOTE: Synthetic Minority Over-sampling Technique. In *Journal of Artificial Intelligence Research* (Vol. 16).

Choubin, B., Borji, M., Mosavi, A., Sajedi-Hosseini, F., Singh, V. P., & Shamshirband, S., 2019. Snow avalanche hazard prediction using machine learning methods. *Journal of Hydrology*, *577*(May), 123929. https://doi.org/10.1016/j.jhydrol.2019.123929.

Chueca Cía, J., Andrés, A. J., & Montañés Magallón, A., 2014. A proposal for avalanche susceptibility mapping in the Pyrenees using GIS: the Formigal-Peyreget area (Sheet 145-I; scale 1:25.000). *Journal of Maps, 10(2)*, 203-210. https://doi.org/10.1080/17445647.2013.870501.

Fazzini, M., Cordeschi, M., Carabella, C., Paglia, G., Esposito, G., & Miccadei, E., 2021. Snow Avalanche Assessment in Mass

Movement-Prone Areas: Results from Climate Extremization in Relationship with Environmental Risk Reduction in the Prati di Tivo Area (Gran Sasso Massif, Central Italy). *Land*, *10*(11), 1176. https://doi.org/10.3390/land10111176.

Hafner, E., & Bühler, Y., 2019. *SPOT6 Avalanche outlines 24 January 2018*. EnviDat. https://doi.org/http://dx.doi.org/10.16904/envidat.77.

Kim, S.-M., & Park, H.-D., 2017. Analogy between grid-based modeling of landslide and avalanche using GIS with surface flow analysis. Bulletin of Engineering Geology and the Environment, 78(1), 189-206. https://doi.org/10.1007/s10064-017-1144-y.

Meseșan, F., Man, T. C., Pop, O. T., & Gavrilă, I. G., 2019. Reconstructing snow-avalanche extent using remote sensing and dendrogeomorphology in Parâng Mountains. Cold Regions Science and Technology, 157, 97-109. https://doi.org/10.1016/j.coldregions.2018.10.002.

Pedregosa, F., Grisel, O., Weiss, R., Passos, A., Brucher, M., Varoquax, G., Gramfort, A., Michel, V., Thirion, B., Grisel, O., Blondel, M., Prettenhofer, P., Weiss, R., Dubourg, V., & Brucher, M., 2011. Scikit-learn: Machine Learning in Python. *Journal of Machine Learning Research*, *12*, 2825–2830.

Pistocchi, A., & Notarnicola, C., 2013. Data-driven mapping of avalanche release areas: A case study in South Tyrol, Italy. *Natural Hazards*, 65(3), 1313–1330. https://doi.org/10.1007/s11069-012-0410-3.

Rahmati, O., Ghorbanzadeh, O., Teimurian, T., Mohammadi, F., Tiefenbacher, J. P., Falah, F., Pirasteh, S., Ngo, P. T. T., & Bui, D. T., 2019. Spatial modeling of snow avalanche using machine learning models and geo-environmental factors: Comparison of effectiveness in two mountain regions. *Remote Sensing*, *11*(24). https://doi.org/10.3390/rs11242995.

Schweizer, J., Jamieson, J. B., & Schneebeli, M., 2003. Snow avalanche formation. *Reviews of Geophysics*, *41*(4). https://doi.org/10.1029/2002RG000123.

Swisstopo., 2021. *Online maps & data*. https://www.swisstopo.admin.ch/en/maps-data-online.html.

Tiwari, A., G., A., & Vishwakarma, B. D., 2021. Parameter importance assessment improves efficacy of machine learning methods for predicting snow avalanche sites in Leh-Manali Highway, India. *Science of the Total Environment*, *794*. https://doi.org/10.1016/j.scitotenv.2021.148738.

Wen, H., Wu, X., Liao, X., Wang, D., Huang, K., & Wünnemann, B., 2022. Application of machine learning methods for snow avalanche susceptibility mapping in the Parlung Tsangpo catchment, southeastern Qinghai-Tibet Plateau. *Cold Regions Science and Technology*, *198*. https://doi.org/10.1016/j.coldregions.2022.103535.

APPENDIX

FACTORS			MEAN	STD	MIN	25%	50%	75%	MAX
Elevation	Inventory -A	Non-avalanche	2022.718	505.606	453.632	1684.412	2072.872	2410.474	3237.224
		Avalanche	2076.937	381.084	856.656	1808.086	2084.501	2352.096	3209.036
	Inventory -B	Non-avalanche	2019.035	503.677	453.632	1680.311	2065.898	2406.594	3237.224
		Avalanche	2137.147	349.738	1078.695	1888.180	2136.086	2385.470	3209.036
Slope	Inventory -A	Non-avalanche	33.821	14.979	0.000	23.940	33.590	42.688	86.979
		Avalanche	33.467	12.868	0.000	25.143	33.131	40.300	85.321
	Inventory -B	Non-avalanche	33.508	14.990	0.000	23.453	33.265	42.369	86.979
		Avalanche	36.968	11.481	0.000	29.896	35.591	42.785	85.321
Aspect	Inventory -A	Non-avalanche	183.858	108.067	-1.000	92.180	184.257	281.686	360.000
		Avalanche	153.513	75.167	-1.000	103.181	150.667	197.542	359.994
	Inventory -B	Non-avalanche	182.901	107.500	-1.000	92.224	182.586	279.147	360.000
		Avalanche	154.661	73.836	-1.000	106.980	153.135	196.755	359.994
Profile Curvature	Inventory -A	Non-avalanche	0.002	7.315	-317.300	-2.067	0.034	2.190	325.558
		Avalanche	0.379	5.811	-193.240	-1.720	0.247	2.186	203.003
	Inventory -B	Non-avalanche	0.010	7.235	-317.300	-2.026	0.041	2.160	325.558
		Avalanche	0.413	6.392	-193.240	-2.011	0.271	2.485	203.003
Plan Curvature	Inventory -A	Non-avalanche	0.093	5.056	-281.991	-1.447	-0.002	1.478	294.960
		Avalanche	-0.344	4.267	-173.432	-1.669	-0.199	1.113	188.452
	Inventory -B	Non-avalanche	0.085	5.004	-281.991	-1.430	-0.007	1.447	294.960
		Avalanche	-0.391	4.676	-173.432	-1.967	-0.251	1.301	188.452
Diurnal Anisotropic Heating	Inventory -A	Non-avalanche	-0.018	0.404	-0.974	-0.356	-0.024	0.325	0.973
		Avalanche	0.126	0.367	-0.938	-0.150	0.175	0.426	0.960
	Inventory -B	Non-avalanche	-0.016	0.401	-0.974	-0.350	-0.019	0.321	0.973
		Avalanche	0.151	0.389	-0.938	-0.146	0.239	0.469	0.960
Slope Length Factor	Inventory -A	Non-avalanche	12.148	6.223	0.000	8.274	12.007	15.441	172.068
		Avalanche	13.989	6.301	0.000	10.267	13.196	16.744	104.631
	Inventory -B	Non-avalanche	12.113	6.228	0.000	8.220	11.959	15.405	172.068
		Avalanche	14.988	5.981	0.000	11.360	13.906	17.475	83.772
Relative Slope Position Index	Inventory -A	Non-avalanche	-4.102	668.904	0.000	0.035	0.246	0.705	16080.000
		Avalanche	-4.870	713.527	0.000	0.006	0.070	0.368	51.291
	Inventory -B	Non-avalanche	-4.151	671.935	0.000	0.029	0.229	0.691	16080.000
		Avalanche	-4.549	694.501	0.000	0.021	0.142	0.480	51.291
Topographic Position Index	Inventory -A	Non-avalanche	0.643	14.025	-129.677	-5.978	-0.696	5.462	231.357
		Avalanche	-4.964	11.038	-96.581	-9.522	-4.065	0.099	109.060
	Inventory -B	Non-avalanche	0.503	13.902	-129.677	-6.034	-0.819	5.220	231.357
		Avalanche	-5.178	12.030	-96.581	-10.485	-4.355	0.589	109.060
Topographic Ruggedness Index	Inventory -A	Non-avalanche	5.341	4.548	0.000	2.987	4.397	6.215	191.151
		Avalanche	4.994	3.644	0.000	3.095	4.286	5.684	124.736
	Inventory -B	Non-avalanche	5.276	4.517	0.000	2.921	4.344	6.141	191.151
		Avalanche	5.633	3.760	0.000	3.765	4.712	6.249	124.736
Topographic Wetness Index	Inventory -A	Non-avalanche	5.690	2.056	-0.634	4.277	5.495	6.792	24.869
		Avalanche	6.446	1.944	0.467	5.157	6.344	7.576	18.466
	Inventory -B	Non-avalanche	5.752	2.089	-0.634	4.311	5.549	6.880	24.869
		Avalanche	5.977	1.644	0.467	4.871	5.951	7.010	16.082
Valley Depth	Inventory -A	Non-avalanche	130.806	118.260	-222.702	33.650	93.546	205.858	573.546
		Avalanche	178.456	122.971	-48.971	74.487	159.891	267.324	569.177
	Inventory -B	Non-avalanche	134.620	120.696	-222.702	34.745	96.957	213.554	573.546
		Avalanche	149.982	106.071	-23.466	61.819	134.019	220.390	562.334
Convergence Index	Inventory -A	Non-avalanche	0.186	5.633	-95.105	-1.958	0.003	1.996	93.177
		Avalanche	-1.382	4.365	-88.141	-3.072	-0.908	0.891	67.722
	Inventory -B	Non-avalanche	0.129	5.632	-95.105	-1.995	-0.023	1.961	93.177
		Avalanche	-1.243	4.035	-70.980	-2.986	-0.896	0.900	54.717
Wind Exposition Index	Inventory -A	Non-avalanche	1.057	0.106	0.770	0.983	1.056	1.130	1.342
		Avalanche	1.044	0.083	0.800	0.986	1.045	1.100	1.328
	Inventory -B	Non-avalanche	1.055	0.106	0.770	0.980	1.054	1.128	1.342
		Avalanche	1.062	0.073	0.810	1.011	1.059	1.110	1.328
Mid-Slope Position Index	Inventory -A	Non-avalanche	0.531	0.293	0.000	0.279	0.545	0.794	1.000
		Avalanche	0.535	0.292	0.000	0.284	0.554	0.797	0.999
	Inventory -B	Non-avalanche	0.537	0.294	0.000	0.285	0.554	0.802	1.000
		Avalanche	0.469	0.275	0.000	0.233	0.464	0.701	0.997
Normalized Height	Inventory -A	Non-avalanche	0.475	0.302	0.000	0.199	0.471	0.745	1.000
		Avalanche	0.332	0.254	0.000	0.112	0.276	0.512	0.997
	Inventory -B	Non-avalanche	0.466	0.304	0.000	0.185	0.457	0.737	1.000
		Avalanche	0.392	0.249	0.001	0.181	0.356	0.577	0.997

Table A1. Summary statistics of the numerical factors based on Inventory-A and Inventory-B.

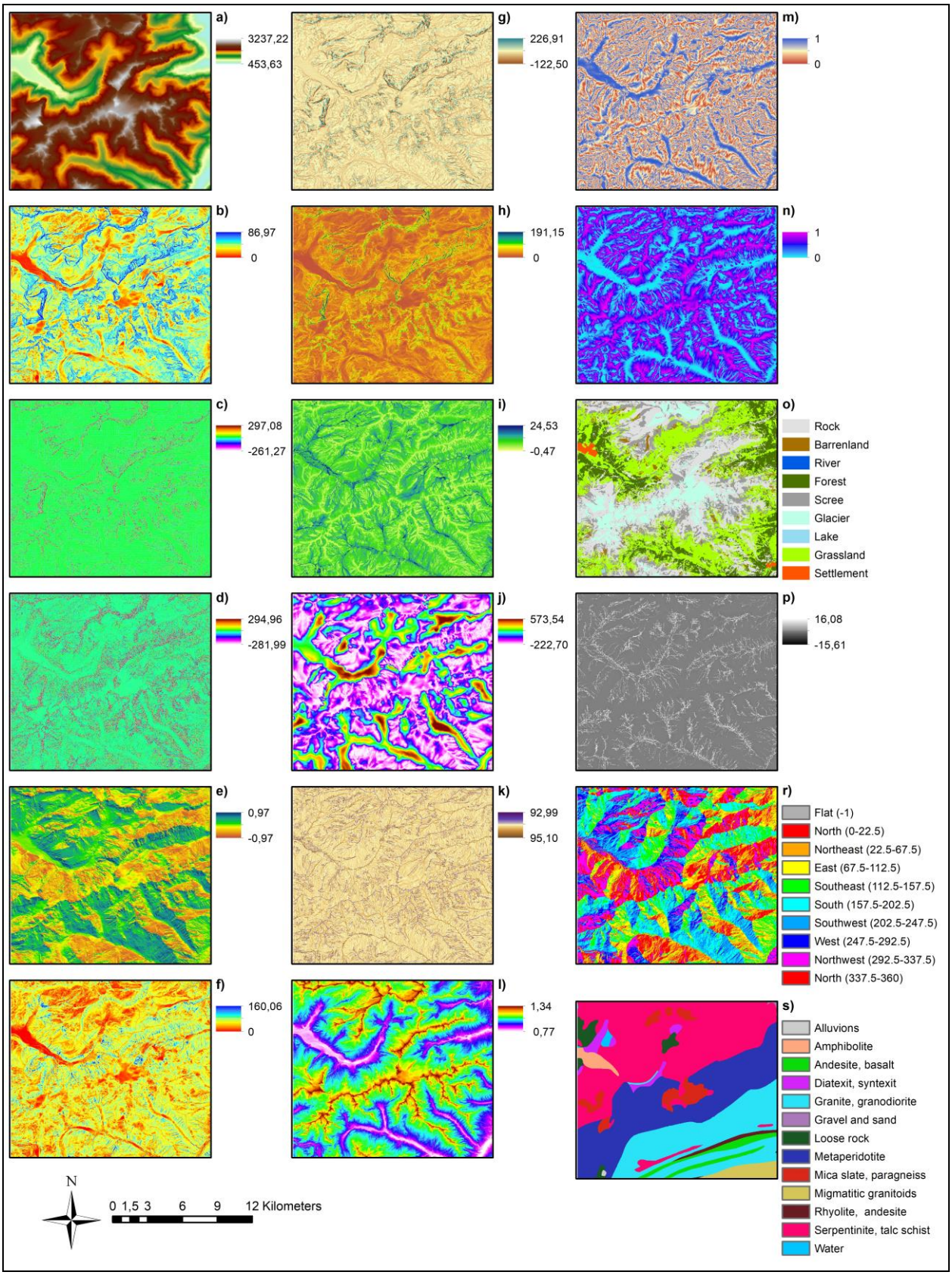

Figure A1. Conditioning factors: a) elevation, b) slope, c) profile curvature, d) plan curvature, e) diurnal anisotropic heating index, f) slope length factor, g) topographic position index, h) topographic ruggedness index, i) topographic wetness index, j) valley depth, k) convergence index, l) wind exposition index, m) mid-slope position index, n) normalized height, o) land use and land cover, p) relative slope position index, r) aspect, s) lithology.